Mechanical Properties of Single and Polycrystalline Solids from Machine Learning

Faridun N. Jalolov, Evgeny V. Podryabinkin, Artem R. Oganov, Alexander V. Shapeev, and Alexander G. Kvashnin*

Calculating the elastic and mechanical characteristics of non-crystalline solids can be challenging due to the high computational cost of ab initio methods and the low accuracy of empirical potentials. This paper proposes a computational technique for efficient calculations of mechanical properties of polycrystals, composites, and multi-phase systems from atomistic simulations with high accuracy and reasonable computational cost. The calculated elastic moduli of polycrystalline diamond and their dependence on grain size are determined using a developed approach based on actively learned machine learning interatomic potentials (MLIPs). These potentials are trained on local fragments of the polycrystalline system, and ab initio calculations are used to compute forces, stresses, and energies. This technique allows researchers to perform extensive calculations of the mechanical properties of complex solids with different compositions and structures, achieving high accuracy and facilitating the transition from ideal (single crystal) systems to more realistic ones.

1. Introduction

Diamond is a widely used material in the manufacturing industry due to its unique properties, particulary its unsurpassed hardness (varying from 60 to 120 GPa[1–4] depending on conditions). Synthetic diamonds, mainly used in industry, are usually synthesized in a polycrystalline structure. The size of crystallites (grains) in diamonds can vary from a few nanometers to tens of microns, depending on the method of production and parameters of the technological process.[5] The mechanical properties of polycrystalline diamond depend on the size of the grains.[6] When the grains are large (about one micron), the specific volume of inter-grain boundaries is not significant and the basic mechanical properties of such diamonds are similar to those of single crystals. However, the specific volume of inter-granular boundaries increases as the grain size decreases, which significantly affects the mechanical properties of diamonds. Huang and Irifune,[7,8] have shown that the elastic properties of polycrystalline diamond may even exceed those of single-crystal diamond. Understanding the relationship between grain size and the properties of polycrystalline diamond is crucial, particularly in the synthesis of polycrystalline diamonds from ultrafine diamond dust. This study aims to comprehensively and accurately investigate the impact of grain size on their mechanical properties in polycrystalline diamonds.

Perhaps the most appropriate approach to studying this problem is to simulate the system at the atomistic level. However, selecting a model for interatomic interaction is crucial. Two traditional approaches for such models are empirical potentials and ab initio calculations. Empirical potentials are used to simulate large atomistic systems due to their computational efficiency. These models have a fixed functional form that is constructed with insight and include only a few fitting parameters, which are chosen to replicate the fundamental properties of single crystals and experimental results in simulations. The commonly used empirical potentials for diamond include the Tersoff potential,[9] the Brenner potential,[10] and the ReaxFF force field,[11] each with its unique characteristics. However, it is important to note that empirical potentials may not accurately reproduce the complex interactions within inter-granular boundaries. This is because the structure in these regions differs from the regular crystal lattice that these potentials have been fitted for.

Erohin et al.[12] conducted a theoretical study on the ultrahigh hardness of polycrystalline diamonds using molecular dynamics simulations with the Brenner potential.[10] The authors analyzed the evolution of the bulk modulus with grain size and identified structures with a higher bulk modulus than that of single crystal diamond. While the use of classical empirical potentials to describe new atomic configurations in polycrystals is debatable, this study suggests that the unusually high bulk modulus may be caused by the anisotropic response of particular grains to hydrostatic stress. This hardening mechanism seems plausible, given its agreement with experimental data.

Density Functional Theory (DFT)[13,14] is the most commonly used quantum-mechanical method for describing material properties. DFT provides highly accurate calculations of energies and forces, but it is only practical for atomistic systems containing several hundred atoms, making it unsuitable for characterizing inter-granular boundaries.

F. N. Jalolov, E. V. Podryabinkin, A. R. Oganov, A. V. Shapeev,
A. G. Kvashnin
Skolkovo Institute of Science and Technology
Skolkovo Innovation Center
Bolshoy Boulevard 30, bld. 1, Moscow 121205, Russia
E-mail: a.kvashnin@skoltech.ru

The ORCID identification number(s) for the author(s) of this article can be found under https://doi.org/10.1002/adts.202301171

**ADVANCED
SCIENCE NEWS**

www.advancedsciencenews.com

**ADVANCED
THEORY AND
SIMULATIONS**

www.advtheorysimul.com

Recently, there has been a rapid development and increased popularity of machine learning-based models for interatomic interaction. These models aim to combine the computational efficiency of empirical potentials with the accuracy of quantum-mechanical models. Machine-learning interatomic potentials (MLIPs) have a flexible functional form that allows for the approximation of any potential energy surface with a predetermined accuracy by increasing the number of parameters. MLIPs use different representations of crystal structures, such as GAP,[15] MTP,[16] NNP[17,18] etc. The use of machine learning (ML) techniques in atomistic simulation of materials has gained significant momentum in recent decades.[17,19–34] Potential parameters are typically identified during the training process to minimize the deviation between predicted and first-principles-calculated forces and energies for configurations in the training set. However, if the atomistic configuration used for energy and forces calculations differs significantly from those in the training set, extrapolation occurs, which may result in an unacceptably high prediction error. To address this issue, MLIPs must be able to identify configurations where extrapolation may occur. This can be achieved through a "learning on-the-fly" approach as proposed by Podryabinkin et al.[35] This method guarantees that there is no extrapolation when computing the energy or forces for atomistic configurations. Zhang et al.[36] propose the Deep Potential GENerator (DP-GEN) "on-the-fly" learning procedure. This model is capable of generating uniformly accurate deep learning-based potential energy surface (PES) models in a way that minimizines human intervention and computational costs for data generation and model training.

Here, we present an active learning method for MLIPs that automatically constructs local configuration fragments. These fragments allow for the extrapolation to a periodic configuration with regular periodic joints. The size of these configurations is small enough to be suitable for DFT calculations. The main objectives of this work are: 1) to investigate the dependence of the elastic properties of polycrystalline diamond on grain size with an accuracy close to that of DFT, and 2) to assess the effectiveness of the active learning method in handling local environments and transforming them into periodic configurations.

2. Experimental Section

2.1. Machine Learning Interatomic Potentials

The development and proliferation of MLIPs had revolutionized computational materials science. MLIPs made it possible to address problems that were previously considered intractable or too resource-intensive. In particular, MLIPs facilitate the simulation of systems with a large number of atoms and problems that require the calculation of physical properties for a large number of systems within a reasonable timeframe.

In particular, MLIPs had enabled the calculation of nanohardness for various materials based on first principles,[37] high-throughput screening, and the acceleration of crystal structure prediction,[35,38] as well as the execution of extended molecular dynamics simulations.[39]

In this work, the Moment Tensor Potentials (MTPs)[16] was used as an interatomic interaction model. MTPs belonged to the class of local machine-learning potentials, where the total energy

of the configuration was composed of the contributions V of individual atoms (site energies) as

$$E^{\text{mtp}}(\text{cfg}) = \sum_{i=1}^{n} V(\mathfrak{n}_i) \tag{1}$$

The site energy of the atom i depends on a local atomic neighborhood $\mathfrak{n}_i = z_i, z_j, \mathbf{r}_{ij}$, which is determined by the type of the central atom z_i, by the types z_j, and the relative positions $\mathbf{r}_{ij} = \mathbf{r}_j - \mathbf{r}_i$ of neighboring atoms within the cut-off radius $\mathbf{r}_j - \mathbf{r}_i \leq R_{\text{cut}}$. The site energies $V(\mathfrak{n}_i)$ are calculated as a linear combination of the basis functions $B_\alpha(\mathfrak{n}_i)$

$$V(\mathfrak{n}_i) = \sum_\alpha \xi_\alpha B_\alpha(\mathfrak{n}_i) \tag{2}$$

The coefficients ξ_α of this linear combination were the subset of the parameters of the potential and are found in the training procedure.

The definition of the basis functions is based on the moment tensor descriptors:

$$M_{\mu,\nu}(\mathfrak{n}_i) = \sum_j f_\mu(|r_{ij}|, z_i, z_j) \underbrace{\mathbf{r}_{ij} \otimes \ldots \otimes \mathbf{r}_{ij}}_{\nu \text{ times}} \tag{3}$$

here $\underbrace{\mathbf{r}_{ij} \otimes \ldots \otimes \mathbf{r}_{ij}}_{\nu \text{ times}}$ is a tensor of rank ν,

$$f_\mu(|\mathbf{r}_{ij}|, z_i, z_j) = \sum_{\beta=1}^{N_Q} c_{\mu,z_i,z_j}^{(\beta)} Q^{(\beta)}(|r_{ij}|) \tag{4}$$

is a scalar radial function, where $\left\{ c_{\mu,z_i,z_j}^{(\beta)} \right\}$ is the set of "radial" parameters,

$$Q^{(\beta)}(|r_{ij}|) = \begin{cases} \varphi^{(\beta)}(|r_{ij}|)(R_{\text{cut}} - |r_{ij}|)^2 & |r_{ij}| < R_{\text{cut}} \\ 0 & |r_{ij}| \geq R_{\text{cut}} \end{cases} \tag{5}$$

are the radial basis function $\left\{ c_{\mu,z_i,z_j}^{(\beta)} \right\}$, based on the Chebyshev polynomials $\varphi^{(\beta)}$. $B_\alpha(\mathfrak{n}_i)$ are constructed from $M_{\mu,\nu}(\mathfrak{n}_i)$ as various convolutions of the tensors of different ranks yielding a scalar. In addition to the energy of the configurations, the implementation of the MTP allowed the calculation of the forces on the atoms and the virial stresses of the configuration based on the analytical derivatives of E with respect to the positions of the atoms.

The parameters of the radial functions $\left\{ c_{\mu,z_i,z_j}^{(\beta)} \right\}$ together with the linear parameters ξ_α form a set of parameters θ of the MTP, which were found in the training procedure. This procedure minimized the standard deviation between the energies, forces, and stresses computed by DFT and MTP over a set of configurations (training set):

$$c \sum_{k=1}^{K} \left[w_e \left(E^{\text{mtp}}(\text{cfg}_k; \theta) - E^{\text{dft}}(\text{cfg}_k) \right)^2 \right.$$

$$\left. + w_f \sum_{i=1}^{N_k} \left| \mathbf{f}_i^{\text{mtp}}(\text{cfg}_k; \theta) - \mathbf{f}_i^{\text{dft}}(\text{cfg}_k) \right|^2 \right. \tag{6}$$

$$+w_s \left| \sigma^{\text{mtp}}(\text{cfg}_k; \theta) - \sigma^{\text{dft}}(\text{cfg}_k) \right|^2 \right] \to \min_{\theta} \qquad (7)$$

The second-order Newton's method is used as a minimization algorithm.

2.2. Active Learning On-The-Fly with Local Atomistic Environments

Arguably, one of the main challenges in using MLIPs was related to their transferability. MLIPs calculated energies and forces by interpolating these quantities over the training set. Therefore, it was crucial that the training set comprehensively covers the configuration space where energy and forces were to be calculated to avoid extrapolation, which inevitably results in predictions of notably low accuracy.

For example, a MLIP that was trained only on bulk configurations may face difficulties when calculating energies and forces at a free surface. Therefore, the use of MLIPs required a mechanism for identifying such extrapolations, which was commonly known as active learning methods. When an extrapolation was identified, the corresponding configuration could be computed using density functional theory (DFT) and then added to the training set. This process expands the training domain, preventing further extrapolation by the MLIP.

It was important to note that during molecular dynamics (MD) simulations, the trajectory may extend beyond the boundaries of the training set, even if no extrapolation was apparent in the initial part of the MD trajectory. Therefore, one of the most efficient methods of using MLIPs was to conduct MD simulations with extrapolation control and dynamically update the potential during the simulation. This practice was often referred to as 'learning on-the-fly'.

Various MLIPs had their own methods for recognizing extrapolations. For instance, MLIPs based on Gaussian Processes, as such a mechanism, use prediction variation estimation.[40] Neural network-based MLIPs, detect extrapolation based on monitoring model committee disagreement.[41] For MTPs, the degree of extrapolation was calculated from the principle of the maximum volume of the domain in the configuration space spanned by the training set and was computed with the MaxVol algorithm.[42] The degree of extrapolation could be estimated for the whole configuration, as well as for atomistic neighborhoods $\mathfrak{n}$ of individual atoms.[43] The second method allowed one to detect local fragments of the configuration with potentially low accuracy of force calculations. This was particularly useful when working with configurations containing large numbers of atoms. However, the problems arise here with the obtaining of ab initio data due to the practical impossibility of calculating large configurations with DFT. This problem could be solved by somehow cutting out the extrapolation fragments from a large configuration, with the number of atoms suitable for DFT calculations (in practice, usually not more than a few hundred atoms).

In recent papers[37,44] the extrapolated atomistic environments were simply cut out and further computed as non-periodic atom clusters. Such an approach was reasonable when dealing with free surfaces within the simulated system. However, in the the work only bulk configurations were treated, and training the po-

tential on fragments with a free surface would lead to an unreasonable extension of the training domain to non-relevant areas with a subsequent decrease in the accuracy. Therefore, in this paper, another approach based on the construction of periodic configurations from cut fragments was realized. This is done as follows:

1. The atomistic environments $\mathfrak{n}$ on which MLIP extrapolates was identified (step (1) in **Figure 1**).
2. From the whole configuration, the atoms inside the cube containing the cutoff sphere with the extrapolative environment $\mathfrak{n}$ were cut. The size of the cube could be slightly larger than $2R_{\text{cut}}$ (step (2) in Figure 1).
3. Next, a periodic supercell was constructed with this cube, having cell parameters 0.5 Å larger on each side of the cube than the cut one to avoid the appearance of extremely short interatomic distances after applying periodicity (step (3) in Figure 1).
4. In the resulting periodic configuration, the lattice vectors and positions of all atoms outside the extrapolation sphere were relaxed. The atoms inside the extrapolation sphere remain fixed and did not change their positions, ensuring that the extrapolation environment did not change during relaxation.

Relaxation in the final step involved two steps: 1) a pairwise repulsive potential was used to fix too short interatomic distances, and 2) DFT calculations were performed to determine energies, forces, and stresses. This essentially constructs the periodic joint similar to a regular intergranular boundary within the cell, and eliminates the formation of irrelevant atomistic fragments on it.

3. Computation Details

3.1. Generation of Polycrystalline Structure Samples

The initial step in calculating elastic moduli is to generate periodic polycrystalline samples. To accomplish this, we use the Voronoi tessellation method[45–47] as implemented in Atomsk.[48] This method divides a given periodic domain into a given number of grains with random shapes and orientations.

The computational domain had a cubic shape with dimensions of $4 \times 4 \times 4$ nm^3. By varying the number of grains, we generated several diamond polycrystals with different grain sizes. For instance, in a polycrystalline sample with an average grain volume of 16 nm^3," there are four grains, while in one with an average grain volume of 64 nm^3," there is only one grain. To investigate the relationship between mechanical properties and grain size, we have produced polycrystalline samples with average grain volumes of 16, 21, 30, 40, 50, and 64 nm^3, as depicted in **Figure 2**.

We also conducted tests to assess the convergence of mechanical properties with respect to the size of the simulation box, while maintaining the same average grain size. Specifically, we considered simulation boxes with dimensions of $2 \times 2 \times 2$, $4 \times 4 \times 4$, and $8 \times 8 \times 8$ nm^3.

3.2. Ab Initio Calculations

Density Functional Theory (DFT) was used as a first-principles method to train the MTPs and to validate the results. DFT

**ADVANCED
SCIENCE NEWS**
www.advancedsciencenews.com

**ADVANCED
THEORY AND
SIMULATIONS**
www.advtheorysimul.com
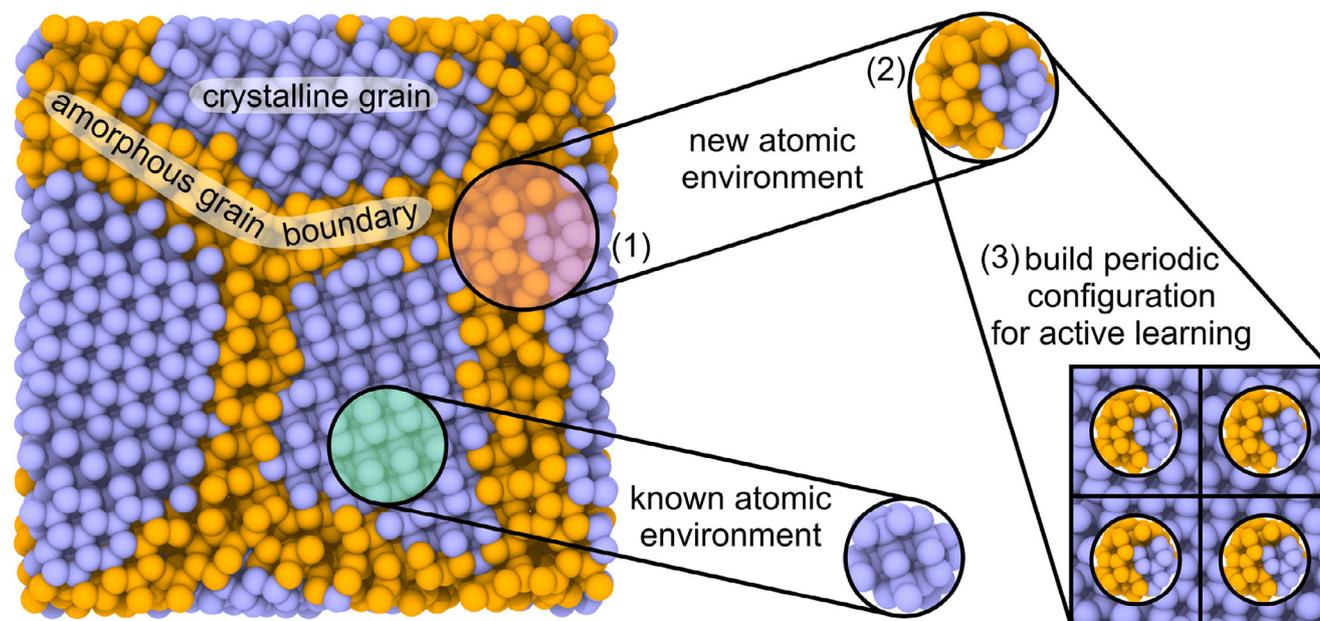
Figure 1. Schematic illustration of learning on the local atomistic environment. The region highlighted by red (1) contains atoms with the highest extrapolative grade, which then cut from the structure (2) and used to build the periodic configuration (3) for further DFT calculations of energy, forces, and stresses.

calculations were performed with the projector augmented-wave density functional theory (PAW-DFT)[14,49] as implemented in the VASP package.[50–53] The generalized gradient approximation with Perdew-Burke-Ernzerhof (GGA-PBE)[54] parametrisation for exchange-correlation functional was used. For each considered single crystal the PAW potentials according to the corresponding number of valence electrons were used to describe the electron-ion interactions. The plane-wave energy cutoff of 500 eV and the Methfessel-Paxton[55] smearing of the electronic occupations ensured the convergence of the total energies. The Γ-centered k-point mesh of $8 \times 8 \times 8$ was used for Brillouin zone sampling. A built-in conjugate gradient method with a maximum net force tolerance of less than 0.01 eVÅ^{-1} was used for potential energy minimization.

For the initial training of our MTP, we actively selected atomistic configurations from ab initio molecular dynamics. The timestep for AIMD was chosen to be equal to 1 fs. The total time of each simulation was 2 ps. The plane wave energy cutoff of 500 eV, the Methfessel–Paxton smearing[55] of the electronic occupations, and Γ-centered k-point meshes with a resolution of $2\pi \times 0.04$ Å^{-1} of the Brillouin zone sampling were used as implemented in VASP.[50–53] These settings ensured the convergence of energy differences and stress tensors. For more details on the training procedure, calculation of MTP forces, the reader was encouraged to check ref. [56].

3.3. Elastic Moduli Calculation

The independent elastic constants for polycrystals were calculated following the standard atomistic simulation methodology as described in ref. [57]. This methodology consists of five steps:

1. Structure relaxation.

2. Applying a finite (approximately 1%) positive and negative strain to the structure in all non-equivalent directions.
3. Relaxation of the strained structure (with the fixed shape of the supercell).
4. Calculation of the stresses for the strained structures.
5. Calculation of the elastic constants using the stresses through finite differences.

The elastic constants C relate the strain ϵ and the stress σ in a linear fashion:

$$\sigma_{ij} = \sum_{kl} C_{ijkl}\epsilon_{kl} \tag{8}$$

For the elastic tensor calculation the Large-scale Atomic/Molecular Massively Parallel Simulator (LAMMPS) package was used.[58]

The elastic moduli values were calculated for various polycrystalline samples with the same average grain size and then averaged. It should be noted that the generated samples are typically non-isotropic and $C_{11} \neq C_{22} \neq C_{33}$, $C_{12} \neq C_{13} \neq C_{23}$, $C_{44} \neq C_{55} \neq C_{66}$. At the same time, a polycrystalline diamond can be considered to be isotropic on a large scale. This allows us to treat C_{22} and C_{33} calculated for the same polycrystalline structure, as additional sampled values for C_{11}. Similarly, C_{13} and C_{23} are the sampled values for C_{12}, and C_{55}, C_{66} are the sampled values for C_{44}. Consequently, elastic constants calculated for a polycrystalline structure give three values each of C_{11}, C_{12}, and C_{44}.

To control for statistical error, we used the k-means method with k = 8. The statistical accumulation process continued until the sample variance of the k-means was greater than 5% of the average value.

**ADVANCED
SCIENCE NEWS**
www.advancedsciencenews.com

**ADVANCED
THEORY AND
SIMULATIONS**
www.advtheorysimul.com
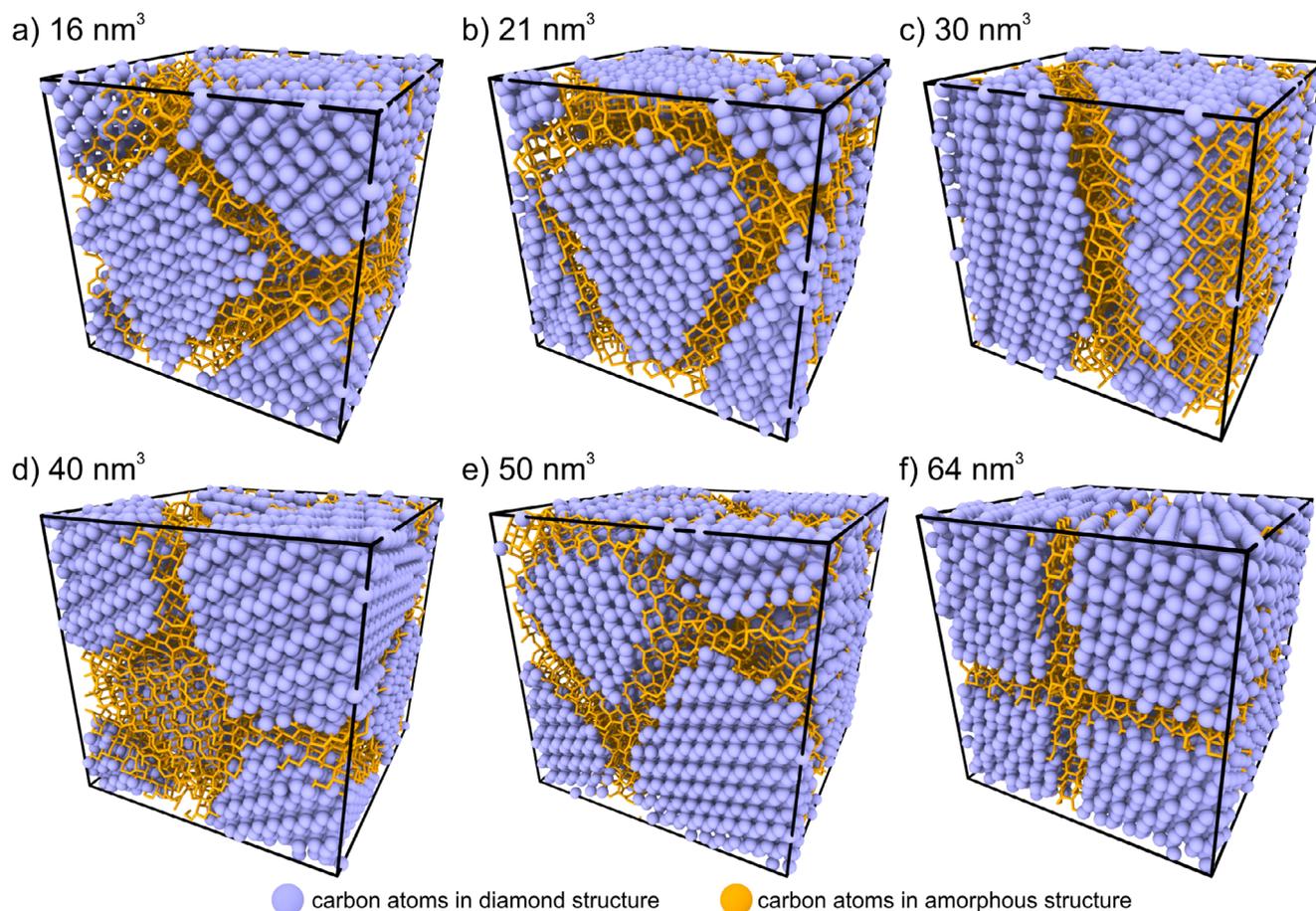
Figure 2. Crystal structure of polycrystals with different grain volumes of a) 16, b) 21, c) 30, d) 40, e) 50, and f) 64 nm^3 produced and considered in our work. The orange and purple colors represent the carbon atoms in amorphous and diamond structure are shown, respectively.

3.4. MTP Construction via Active Learning On-The-Fly

Statistically reliable elastic moduli values are averaged from the values calculated for dozens or even hundreds of samples. The calculation of elastic moduli for each sample assume a number of deformations and applying of relaxation procedures to the sample structure. Thus, energy, forces and stresses are evaluated with MTP for atomistic configurations at each step of the deformation-relaxation procedure. Some of these configurations may have local fragments where MTP extrapolates. In our active learning on-the-fly scheme, we evaluate the degree of extrapolation for each atomic environment in each configuration. If the extrpolation degree exceeds some critical value, the extrpolation fragment is processed with DFT and learned. This procedure is shown schematically in **Figure 3**.

However, on-the-fly active learning of the MTP from scratch is not computationally efficient. Therefore, we pre-trained our MTP passively manner with the atomistic configurations sampled from ab initio molecular dynamics trajectories (step 1 in Figure 3). For this purpose we perform ab initio molecular dynamics with DFT on 64 atoms of two-grain diamond over 1 ps (1000 timesteps).
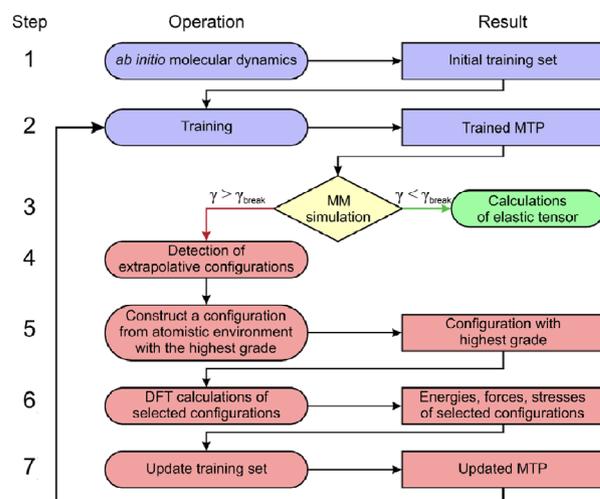
Figure 3. Developed an active learning bootstrapping iteration scheme for the calculations of mechanical properties of crystalline and non-crystalline solids.

**ADVANCED
SCIENCE NEWS**

www.advancedsciencenews.com

**ADVANCED
THEORY AND
SIMULATIONS**

www.advtheorysimul.com
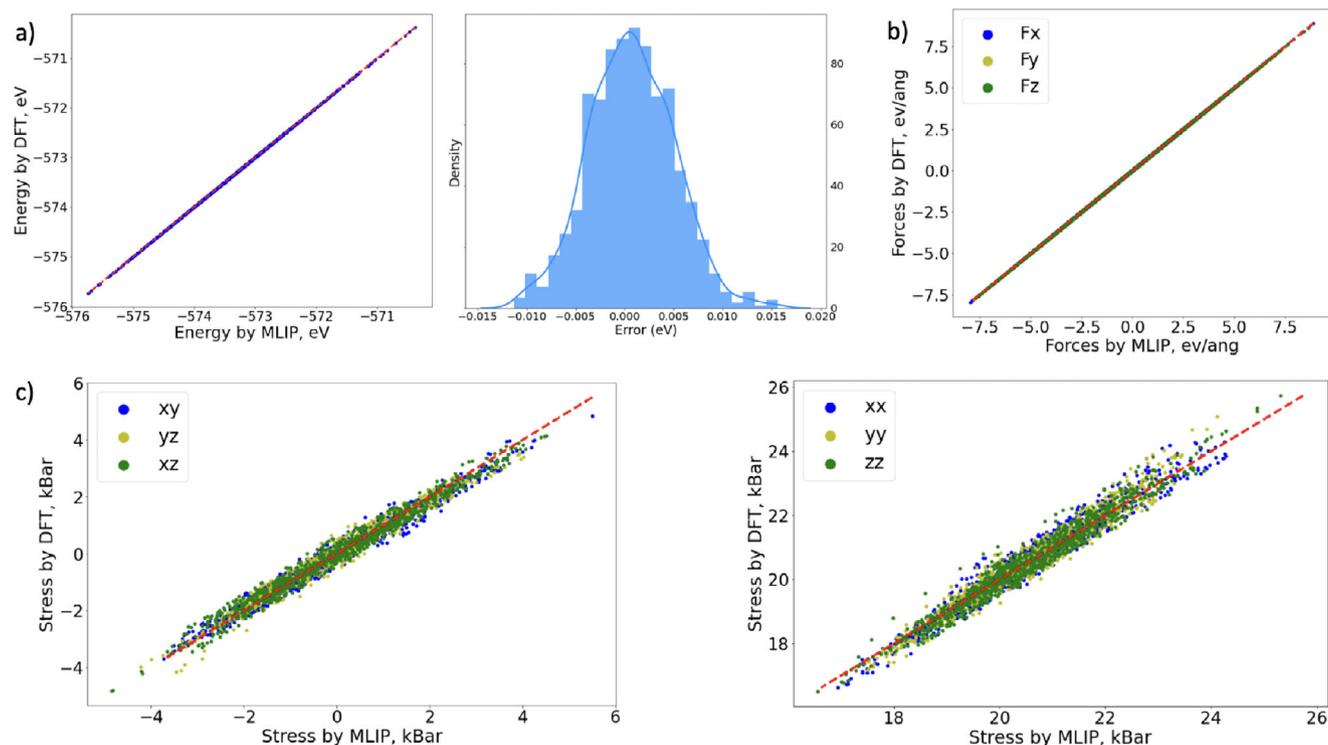
Figure 4. Calculated by DFT and fitted by MTP values of (a) total energy with error distribution, (b) forces, and (c) stresses, obtained for MTP for single crystal diamond.

After the MTP training (step 2 in Figure 3), we started the molecular mechanics (MM) simulation to calculate the elastic tensor for the studied system (steps 3–7 in Figure 3). This process involved the active selection of extrapolative configurations, and the so-called one-extrapolation-threshold scheme ($\mathcal{Y}_{break}$) was used.[56] Exceeding $\mathcal{Y}_{break}$ indicates a very high extrapolation degree and the potential for low accuracy in predicting energy, forces, and stresses. Consequently, we terminate the elastic tensor calculation to retrain MTP. The value of $\mathcal{Y}_{break}$ was set to 11 based on our experience, as it provides an optimal balance between MTP accuracy and retraining frequency. A detailed description of the scheme is described in ref. [56].

After reaching the termination condition ($\mathcal{Y} \leq \mathcal{Y}_{break}$), we select the configurations to be added to the training set from all extrapolated configurations for which the extrapolation was detected (step 4 in Figure 3). A selection procedure is necessary to construct a new active set from a pool of extrapolative configurations.

In the step 5, we extract from the large configuration a cubic box containing the local atomic environments responsible for the extrapolation. The extrapolative atomic environment includes the central atom and its neighborhood in the cutoff sphere, which was taken from 5 Å.

The constructed local atomic structure extracted from polycrystalline material typically contains around 100 atoms. In the next step (step 6), this atomic configuration expanded into a periodic structure with the relaxation performed using DFT for atoms outside the extrapolative environment. This relaxation aims to minimize the energy of the periodic interface. Simultaneously, DFT calculations of energy, forces, and stresses are performed.

Further steps of adding to the initial training set with subsequent retraining of MTP (steps 7 and 2 in Figure 3). The use of this scheme eliminates the need to consider the entire polycrystalline structure in the DFT calculations for the actively learn MTP. Thus, once the first iteration of active learning of the MTP has been completed, the MD simulation of the elastic tensor can be continued with updated actively learned MTP until the critical value of extrapolation is reached again or the calculation of all configurations is completed. Each iteration of this scheme expands the training domain and improves the transferability of the MTP (i.e., the number of extrapolations and the extrapolation degree are reduced). As was discussed above, a similar approach has recently been used in ref. [37] to simulate the nanohardness of single crystal compounds and in an MD run for copper.[44]

The MTPs for single crystals has been applied to diamond, Si, SiC, WC, and CrB$_4$. Detailed information on the results for these studied single crystals can be found in Tables S1–S6 (Supporting Information).

4. Results and Discussion

4.1. MTP for Polycrystalline Diamond

The accuracy of the obtained MTP for single crystal diamond, as the base for learning of the MTP for polycrystals has been estimated. The total energies, forces, and stresses as calculated by DFT and MTP for single crystal diamond are presented in **Figure 4**. All the metrics are presented for each configuration in the training set. For the calculated and fitted energies (Figure 4a) the maximal absolute difference is 6.7×10^{-2} eV, the average

**ADVANCED
SCIENCE NEWS**

www.advancedsciencenews.com

**ADVANCED
THEORY AND
SIMULATIONS**

www.advtheorysimul.com
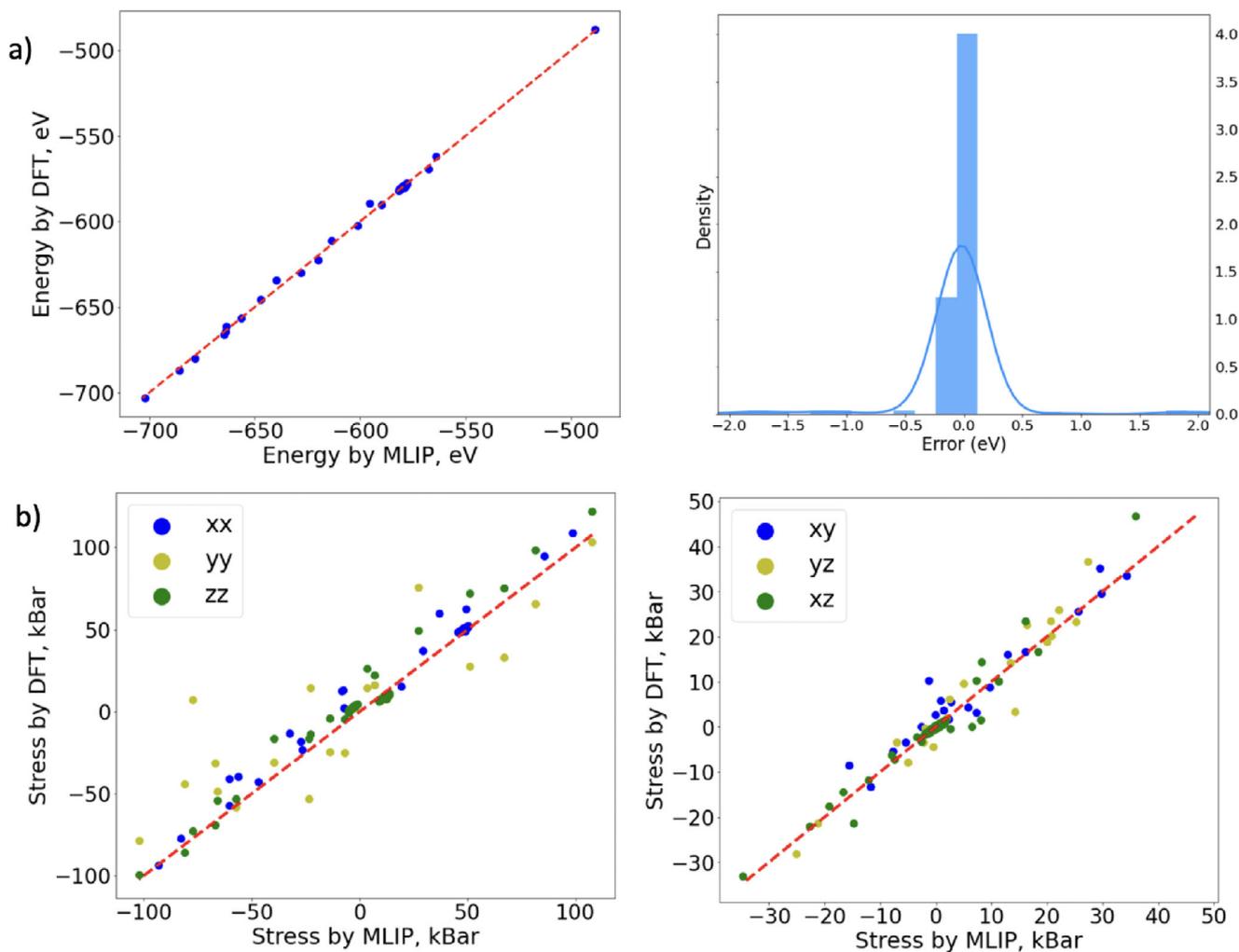
Figure 5. Calculated by DFT and fitted by MLIP values of a) total energy with error distribution and b) stresses only for local configurations extracted from the polycrystal for active learning.

absolute difference is 4.1×10^{-3} eV, and the RMS absolute difference is 7.1×10^{-3} eV. The error distribution shows the correlation between the calculated and fitted energies. It is highly symmetric around zero and can be considered as Gaussian type. From this fact we can conclude that the MTPs have no systematic bias toward the over- or underestimation of the results.

For the calculated and fitted forces (see Figure 4b) the maximal absolute difference, average absolute difference, and RMS absolute difference are 1.3 eVÅ^{-1}, 2×10^{-2} eVÅ^{-1}, and 2.2×10^{-2} eVÅ^{-1} respectively. For stresses we obtained the values of 2.5, 0.7, and 0.7 kBar for the maximal absolute difference, average absolute difference, and RMS absolute difference, respectively, see Figure 4c.

The accuracy of the actively learned MTP on the local atomistic environments for polycrystalline diamond was next estimated. The total energies, forces, and stresses calculated with DFT and MTP for local configurations extracted from the polycrystal are presented in **Figure 5**. For the calculated and fitted energies (Figure 5a) the maximal absolute difference is 7.6×10^{-2}

eV, the average absolute difference is 1.9×10^{-3} eV, and the RMS absolute difference is 7.9×10^{-3} eV. The error distribution shows the relation between the DFT and MTP energies.

Regarding stresses, we obtained the values of 10.7, 2.7, and 3.1 kBar for the maximal absolute difference, average absolute difference, and RMS absolute difference, respectively, see Figure 5b. All the obtained trend lines and calculated absolute differences for energies, forces, and stresses demonstrate an accurate predictive power of used MTP.

4.2. Mechanical Properties of Polycrystalline Diamond

Polycrystals can be considered as orthotropic materials with nine independent second order elastic constants are presented and should be calculated, namely C_{11}, C_{22}, C_{33}, C_{44}, C_{55}, C_{66}, C_{12}, C_{13}, and C_{23}. The elastic moduli were determined by combining these components of the elastic tensor using Voigt-Reuss-Hill averaging. The results of calculations for the elastic moduli of

**ADVANCED
SCIENCE NEWS**

www.advancedsciencenews.com

**ADVANCED
THEORY AND
SIMULATIONS**

www.advtheorysimul.com
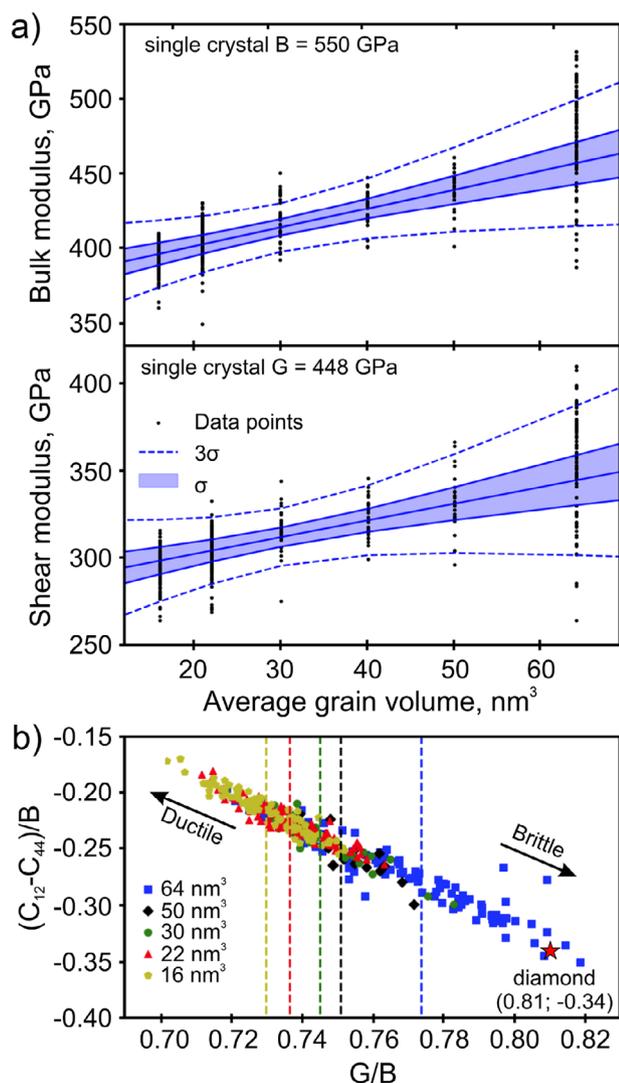
Figure 6. a) Dependence of the bulk (top) and shear (bottom) moduli of diamond polycrystals with different grains sizes compared to the single crystal diamond. b) The correlation between $(C_{12}-C_{44})/B$ and G/B, where B is bulk modulus, G is shear modulus showing the change in ductility and brittleness of polycrystals as a function of grain size. Dashed vertical lines indicate the average values between structures of the same grain size. The value for the diamond is shown by the red star.

polycrystalline diamond with different grain sizes, using actively learned MTP on local environments are shown in **Figure 6**. One can see that the bulk modulus of polycrystalline diamond increases with increasing the average grains size, tending toward the bulk modulus of single crystal diamond as a limiting case (Figure 6a). For each grain size, a number of structures (from 23 to 100) were generated that explain the deviation of the calculated bulk modulus. For each grain size, the sample variance σ and the sample mean M values were calculated. We continued to generate and calculate elastic moduli until the statistical error was reduced to less than 1%.

The average grain sizes for which the diamond polycrystals were generated were selected using a Gaussian Process (GP) with a Radial Basis Function (RBF) kernel. Initially, we simulated

two diamond polycrystals with average grain sizes of 16 and 64 nm^3 and calculated elastic constants for them according to our setup (Figure 3). The results of the bulk modulus calculation of these two polycrystals are shown in Figure S2 (Supporting Information). According to these results, we determined the confidence parameters in the GP to define the grain size for further polycrystals in order to minimize the confidence parameters, see Figure S2 (Supporting Information). Then the other sizes, namely 40, 30, 50, and 22 nm^3 (in this order) were added for consideration to minimize the confidence parameter in the GP.

The results for the bulk modulus of the considered polycrystals show a monotonic growth, starting from 400 GPa (which is close to the value for the amorphous carbon structure) and reaching 480 GPa for the structure with an average grain volume of 64 nm^3, see Figure 6a. The average value of the bulk modulus for the largest grain size polycrystal is about 500 GPa. This value falls below the calculated bulk modulus for single crystal diamond, which is 550 GPa, but it falls within the confidence interval of our calculations. The results of the elastic moduli calculation Figure 6 were fitted by another GP with the kernel given by

$$k(V_1, V_2) = \theta_0^2 + \theta_1^2 V_1 V_2 + \theta_2^2 e^{(V_1-V_2)^2/(2\theta_3^2)} \qquad (9)$$

with V_1, V_2 being the polycrystal sizes and $\theta_0, \dots \theta_3$ being the hyperparameters. This kernel encodes an arbitrary linear dependence given by the first two terms and a correction to the linear dependence given by the last term. The blue area in Figure 6 represents one sigma, and the dashed lines indicate three sigmas. Overall, these results can be interpreted as a smooth, near-linear relationship with a noise.

In order to assess the influence of grain size on the ductility and brittleness of polycrystals, we have calculated the Pugh-Pettifor criterion,[59] as shown in Figure 6b. The correlation between $(C_{12}-C_{44})/B$ and G/B allows us to determine the ductility and brittleness of the polycrystals. As can be seen, polycrystals with small grain sizes (16, 22 nm^3) are more ductile compared to larger grain sizes, see Figure 6b. As the grain size increases, the polycrystals become more brittle. The average G/B ratio for polycrystals with a grain size of 64 nm^3 is approximately 0.775 and the maximum value reaches about 0.82, see Figure 6b. According to these data, the mechanical stiffness of the considered polycrystals does not exceed the value of single crystal diamond (G/B is 0.81). Thus, all considered polycrystals with various grain sizes are less brittle according to the Pugh-Pettifor criterion compared to single crystal diamond.

5. Conclusion

We have developed the active learning bootstrapping iteration scheme for the precise calculation of the elastic tensor in complex solids, namely composites, polycrystals, and multiphase systems, by using machine learning interatomic potentials with active learning on local atomic environments. Our scheme allows one to achieve high accuracy in simulating the elastic properties of complex solids. The proposed scheme has been used to calculate the elastic tensor and elastic moduli both for single crystals with various structures and compositions and polycrystalline structures. To evaluate our approach, diamond polycrystals were

ADVANCED
SCIENCE NEWS

www.advancedsciencenews.com

ADVANCED
THEORY AND
SIMULATIONS

www.advtheorysimul.com

assessed, and the resulting elastic properties were compared with existing reference data, demonstrating excellent conformity and precision. This developed approach allows the study of the mechanical properties of materials that usually synthesized and used in experiments, i.e., noncrystalline materials. This enables comprehensive investigations into the mechanical properties of complex materials, such as polycrystals and composites, bringing the obtained data closer to those found in experiments.

Supporting Information

Supporting Information is available from the Wiley Online Library or from the author.

Conflict of Interest

The authors declare no conflict of interest.

Data Availability Statement

The data that support the findings of this study are available from the corresponding author upon reasonable request.

[1] A. G. Kvashnin, Z. Allahyari, A. R. Oganov, *J. Appl. Phys.* **2019**, *126*, 040901.
[2] R. Andrievski, *Int. J. Refract. Met. Hard Mater.* **2001**, *19*, 447.
[3] J. Field, *Rep. Prog. Phys.* **2012**, *75*, 126505.
[4] V. Blank, M. Popov, G. Pivovarov, N. Lvova, K. Gogolinsky, V. Reshetov, *Diamond Relat. Mater.* **1998**, *7*, 427.
[5] T. A. Scott, *Adv. Appl. Ceram.* **2018**, *117*, 161.
[6] A. Lammer, *Mater. Sci. Technol.* **1988**, *4*, 949.
[7] Q. Huang, D. Yu, B. Xu, W. Hu, Y. Ma, Y. Wang, Z. Zhao, B. Wen, J. He, Z. Liu, Y. Tian, *Nature* **2014**, *510*, 250.
[8] T. Irifune, A. Kurio, S. Sakamoto, T. Inoue, H. Sumiya, *Nature* **2003**, *421*, 599.
[9] J. Tersoff, *Phys. Rev. Lett.* **1988**, *61*, 2879.
[10] D. W. Brenner, O. A. Shenderova, J. A. Harrison, S. J. Stuart, B. Ni, S. B. Sinnott, *J. Phys.: Condens. Matter* **2002**, *14*, 783.
[11] A. C. Van Duin, S. Dasgupta, F. Lorant, W. A. Goddard, *J. Phys. Chem. A* **2001**, *105*, 9396.
[12] S. Erohin, P. Sorokin, *Appl. Phys. Lett.* **2015**, *107*, 12.
[13] L. J. Sham, W. Kohn, *Phys. Rev.* **1966**, *145*, 561.
[14] P. Hohenberg, W. Kohn, *Phys. Rev.* **1964**, *136*, B864.
[15] A. P. Bartók, R. Kondor, G. Csányi, *Phys. Rev. B* **2013**, *87*, 184115.
[16] A. V. Shapeev, *Multiscale Model. Simul.* **2016**, *14*, 1153.
[17] J. Behler, M. Parrinello, *Phys. Rev. Lett.* **2007**, *98*, 146401.
[18] J. Behler, *Phys. Chem. Chem. Phys.* **2011**, *13*, 17930.
[19] A. P. Bartók, M. C. Payne, R. Kondor, G. Csányi, *Phys. Rev. Lett.* **2010**, *104*, 136403.
[20] M. Rupp, A. Tkatchenko, K.-R. Müller, O. A. Von Lilienfeld, *Phys. Rev. Lett.* **2012**, *108*, 058301.
[21] G. Montavon, M. Rupp, V. Gobre, A. Vazquez-Mayagoitia, K. Hansen, A. Tkatchenko, K.-R. Müller, O. A. Von Lilienfeld, *New J. Phys.* **2013**, *15*, 095003.
[22] F. Noé, A. Tkatchenko, K.-R. Müller, C. Clementi, *Annu. Rev. Phys. Chem.* **2020**, *71*, 361.
[23] K. T. Butler, D. W. Davies, H. Cartwright, O. Isayev, A. Walsh, *Nature* **2018**, *559*, 547.
[24] K. T. Schütt, H. E. Sauceda, P.-J. Kindermans, A. Tkatchenko, K.-R. Müller, *J. Chem. Phys.* **2018**, *148*, 24.
[25] P. Friederich, F. Häse, J. Proppe, A. Aspuru-Guzik, *Nat. Mater.* **2021**, *20*, 750.
[26] N. Lopanitsyna, C. B. Mahmoud, M. Ceriotti, *Phys. Rev. Mater.* **2021**, *5*, 043802.
[27] G. Imbalzano, Y. Zhuang, V. Kapil, K. Rossi, E. A. Engel, F. Grasselli, M. Ceriotti, *J. Chem. Phys.* **2021**, *154*, 7.
[28] B. Cheng, E. A. Engel, J. Behler, C. Dellago, M. Ceriotti, *Proc. Nat. Acad. Sci.* **2019**, *116*, 1110.
[29] G. Carleo, I. Cirac, K. Cranmer, L. Daudet, M. Schuld, N. Tishby, L. Vogt-Maranto, L. Zdeborová, *Rev. Mod. Phys.* **2019**, *91*, 045002.
[30] D. Dragoni, T. D. Daff, G. Csányi, N. Marzari, *Phys. Rev. Mater.* **2018**, *2*, 013808.
[31] A. P. Bartók, J. Kermode, N. Bernstein, G. Csányi, *Phys. Rev. X* **2018**, *8*, 041048.
[32] O. Isayev, D. Fourches, E. N. Muratov, C. Oses, K. Rasch, A. Tropsha, S. Curtarolo, *Chem. Mater.* **2015**, *27*, 735.
[33] W. J. Szlachta, A. P. Bartók, G. Csányi, *Phys. Rev. B* **2014**, *90*, 104108.
[34] V. L. Deringer, G. Csányi, *Phys. Rev. B* **2017**, *95*, 094203.
[35] E. V. Podryabinkin, E. V. Tikhonov, A. V. Shapeev, A. R. Oganov, *Phys. Rev. B* **2019**, *99*, 064114.
[36] Y. Zhang, H. Wang, W. Chen, J. Zeng, L. Zhang, H. Wang, W. E, *Comput. Phys. Commun.* **2020**, *253*, 107206.
[37] E. V. Podryabinkin, A. G. Kvashnin, M. Asgarpour, I. I. Maslenikov, D. A. Ovsyannikov, P. B. Sorokin, M. Y. Popov, A. V. Shapeev, *J. Chem. Theory Comput.* **2022**, *18*, 1109.
[38] K. Gubaev, E. V. Podryabinkin, G. L. Hart, A. V. Shapeev, *Comput. Mater. Sci.* **2019**, *156*, 148.
[39] A. V. Shapeev, E. V. Podryabinkin, K. Gubaev, F. Tasnádi, I. A. Abrikosov, *New J. Phys.* **2020**, *22*, 113005.
[40] Y. Zuo, C. Chen, X. Li, Z. Deng, Y. Chen, J. Behler, G. Csányi, A. V. Shapeev, A. P. Thompson, M. A. Wood, S. P. Ong, *J. Phys. Chem. A* **2020**, *124*, 731.
[41] C. Schran, K. Brezina, O. Marsalek, *J. Chem. Phys.* **2020**, *153*, 10.
[42] S. A. Goreinov, I. V. Oseledets, D. V. Savostyanov, E. E. Tyrtyshnikov, N. L. Zamarashkin, in *Matrix Methods: Theory, Algorithms And Applications: Dedicated to the Memory of Gene Golub*, World Scientific, Singapore **2010**, pp. 247–256.
[43] E. V. Podryabinkin, A. V. Shapeev, *Comput. Mater. Sci.* **2017**, *140*, 171.
[44] E. Podryabinkin, K. Garifullin, A. Shapeev, I. Novikov, *J. Chem. Phys.* **2023**, *159*, 084112.
[45] W. Brostow, J.-P. Dussault, B. L. Fox, *J. Comput. Phys.* **1978**, *29*, 81.
[46] J. L. Finney, *J. Comput. Phys.* **1979**, *32*, 137.
[47] M. Tanemura, T. Ogawa, N. Ogita, *J. Comput. Phys.* **1983**, *51*, 191.
[48] P. Hirel, *Comput. Phys. Commun.* **2015**, *197*, 212.

[49] W. Kohn, L. J. Sham, *Phys. Rev.* **1965**, *140*, A1133.

[50] J. Hafner, *J. Comput. Chem.* **2008**, *29*, 2044.

[51] G. Kresse, J. Furthmüller, *Phys. Rev. B* **1996**, *54*, 11169.

[52] G. Kresse, J. Hafner, *Phys. Rev. B* **1993**, *47*, 558.

[53] G. Kresse, J. Hafner, *Phys. Rev. B* **1994**, *49*, 14251.

[54] J. P. Perdew, K. Burke, M. Ernzerhof, *Phys. Rev. Lett.* **1996**, *77*, 3865.

[55] H. J. Monkhorst, J. D. Pack, *Phys. Rev. B* **1976**, *13*, 5188.

[56] I. S. Novikov, K. Gubaev, E. V. Podryabinkin, A. V. Shapeev, *Mach. Learn.: Sci. Technol.* **2020**, *2*, 025002.

[57] S. M. Rassoulinejad-Mousavi, Y. Mao, Y. Zhang, *J. Appl. Phys.* **2016**, *119*, 24.

[58] S. Plimpton, *J. Comput. Phys.* **1995**, *117*, 1.

[59] O. Senkov, D. Miracle, *Sci. Rep.* **2021**, *11*, 4531.